Graphical abstract

○ Synthesized 3-*D* core-shell structured $Ni_3S_2@Co(OH)_2$ composite materials.

○ Combined with wind power generation to electrolyze water.

○ 3-*D* $Ni_3S_2@Co(OH)_2$ controlled synthesis and developed as bifunctional catalyst.

○ A cell voltage of 1.7 V at a current density of 100 $mAcm_{-2}$.

Multidimensional regulation of Ni$_3$S$_2$@Co(OH)$_2$ catalyst with high performance for wind energy electrolytic water

Zining Wang[a], Hui Wang[a], Shan Ji[a,b*], Xuyun Wang[a], Bruno G. Pollet[c], Rongfang Wang[a**]

[a] State Key Laboratory Base for Eco-Chemical Engineering, College of Chemical Engineering, Qingdao University of Science and Technology, Qingdao, 266042, China

[b] College of Biological, Chemical Science and Chemical Engineering, Jiaxing University, Jiaxing, 314001, China

[c] Department of Energy and Process Engineering, Faculty of Engineering, Norwegian University of Science and Technology, NO-7491 Trondheim, Norway

Corresponding authors:

Shan Ji (*): jishan@zjxu.edu.cn, Tel./fax: +86 (572)83643264

Rongfang Wang(**):rfwang@qust.edu.cn, Tel./fax: +86(0)17866858722

50

51
52
53
54
55
56
57
58
59
60
61
62
63
64
65

Abstract:

Combining renewable energy technologies with water electrolyzers to produce green hydrogen should provide a very promising strategy for future sustainable and pollution-free energy supply. In this study, 3-*D* Ni_3S_2@$Co(OH)_2$ nanowires with core-shell structure, which are directly fabricated on nickel (Ni) foam, are developed as a bifunctional catalyst for oxygen evolution reaction (OER) and hydrogen evolution reaction (HER). In such a core-shell structure, the ultrathin α-$Co(OH)_2$ layer of nanosheets (shell) are uniformly wrapped around the Ni_3S_2 nanowires (core). It is found that the obtained 3-*D* Ni_3S_2@$Co(OH)_2$ nanowires could provide large electrochemical surface areas for the electrocatalytic reactions, and further resulted in enhanced electrocatalytic performance. The as-prepared catalyst exhibits a low onset potential and low resistance of charge transfer as well as excellent stability towards the HER. In terms of the onset potential and stability towards the OER, it is observed that the Ni_3S_2@$Co(OH)_2$ is comparable to that of the RuO_2. Due to its well-defined bifunctionality, it is found that an *as*-prepared water electrolyzer with Ni_3S_2@$Co(OH)_2$ as a bifunctional catalyst for HER and OER could deliver a constant cell voltage of 1.64 V at the current density of 10 mA.cm$_{-2}$ for 100 h.

Keywords: 3-*D* core-shell structure; oxygen evolution reaction; hydrogen evolution reaction; bifunctional catalyst; sustainable energy.

3

1. Introduction

Hydrogen (H_2) can be used as a universal energy carrier for stationary and mobile applications. It can be produced in a sustainable and greenway from the water via water electrolyzers powered by the electricity generated by renewable energy systems [1-4]. During water electrolysis, the hydrogen evolution reaction (HER) occurs on the cathode and the oxygen evolution reaction (OER) on the anode [5, 6]. However, costly precious group metal (PGM) catalysts [7, 8] (e.g. Pt and Ir as IrO_2) are usually used to catalyze the HER and OER due to their low anodic and cathodic overpotentials. Thus, to design and develop non-precious metal catalysts has become an active R&D topic in the field of water electrolyzers over the last decade [9].

Transitional-metal-based compounds [10, 11] (TMC), for instance oxides [12, 13], sulphides [14], hydroxides [15, 16], selenides [17, 18], have been extensively investigated as promising alternative materials to the HER and OER PGM electrocatalysts. The layer-structured transition-metal hydroxides are promising HER and OER electrocatalysts due to their cheap price and relatively high activity. Such a layered structure exhibits a large interlayer distance, which can facilitate ion transport and diffusion of reactants during the electrochemical processes [19]. Although great progress has been achieved in the development of HER and OER catalysts based upon TMCs, to date the TMCs still cannot match PGM electrocatalysts in terms of electrocatalytic activity and durability [20].

3

Ultrathin α-Co(OH)$_2$ nanosheets have been developed by Liu *et al.* [21] as HER and OER electrocatalysts. They found that the cathodic and anodic overpotentials for the HER and OER in a KOH electrolyte were +170 mV and +270 mV (at 10 mA cm^{-2}) respectively. Jiang *et al.* also synthesized α-Co(OH)$_2$ nanosheets supported on both polyimide film and carbon as OER electrocatalyst, which exhibited a low overpotential for the OER in alkaline media [22]. However, they found that the HER and OER performance of α-Co(OH)$_2$ nanosheets are greatly influenced by the slow kinetics owing to its poor electrical conductivity [23]. It was also found that Co(OH)$_2$ supported on carbon materials could significantly improve the electrochemical performance. For example, Co(OH)$_2$ supported on carbon fibers and graphene showed enhanced electrochemical performance when compared to the Co(OH)$_2$ alone [24]. However, the high cost of these carbon support materials makes them economically unfeasible for large scale water electrolyzer systems.

Metal sulphides with high theoretical capacitance are recognized as promising electrodes for electrochemical energy storage since they have high electrical conductivity, low cost and high rate capability [25, 26]. Moreover, the development of binary metal sulphides could also further improve the electrochemical properties due to the synergistic effect. Therefore, the use of metal sulphide as support material for the fabrication of core-shell structured α-Co(OH)$_2$@metal sulphide may lead to possible practical interests.

Herein, one-dimensional and low-cost Ni$_3$S$_2$ was developed as a support material for the α-Co(OH)$_2$ nanosheets since Ni$_3$S$_2$ usually possesses higher conductivity than

4

its corresponding oxide [27]. 1-*D* Ni_3S_2 wires were directly formed on the Ni foam, which acted as the current collector, and the interconnected nanowires formed a 3-*D* network. Subsequently, 2-*D* α-$Co(OH)_2$ shell was fabricated on the surface of 1-*D* Ni_3S_2 nanowires to form $Ni_3S_2@Co(OH)_2$ composite with core-shell structure. The obtained $Ni_3S_2@Co(OH)_2$ composite material demonstrated good electrochemical activity towards both the HER and OER due to the synergetic effect of Ni_3S_2 and $Co(OH)_2$ as well as the unique hierarchical structure.

2. Experimental Methods

2.1 Synthesis of core-shell structured $Ni_3S_2@Co(OH)_2$

Before growing 1-D Ni_3S_2 nanowires on Ni foam, the Ni foam had to be pre-treated in an acid solution. The detailed procedure is as follows: Ni foam (size: 3 cm × 2 cm) was put in aqueous HCl solution (1 M) and ultrasonicated for 10 min, and then rinsed thoroughly by ultrapure water. The treated Ni foam was vacuum-dried at 40 °C for further use. A solvothermal method was employed to fabricate the Ni_3S_2 nanowires directly on Ni foam and detailed procedure is as follows: 16 absolute ethylalcohol (16 ml) and anhydrous ethanediamine (16 ml) were mixed together by stirring. Sulfur powder (2 mmol) was introduced to the above solution with magnetic stirring. The obtained mixture was transferred into an autoclave (Teflon-lined) and the Ni foam was put on the bottom of the autoclave and then heat-treated at 160 °C for 6 h. Once the autoclave was cooled to ambient temperature, the Ni foam was rinsed by water and ethanol alternatively, and vacuum-dried again at 40 °C. The final product was

denoted as Ni_3S_2. The mass loading of Ni_3S_2 is 4.8 mg cm-2. Subsequently,

$CoCl_2 \cdot 6H_2O$ (1 mmol) and hexamethylenetetramine (0.5 mmol) were dissolved in

water (40 ml). The obtained mixture and Ni_3S_2 materials were transfered into the

autoclave again and heated at 90 °C for 5 h. The obtained sample was washed

thoroughly with water and then dried in a vacuum oven at 40 °C for 12 h. The final

sample was denoted as $Ni_3S_2@Co(OH)_2$. The mass loading of $Ni_3S_2@Co(OH)_2$ on Ni

foil is 6.1 mg cm-2. For comparison purposes, $Co(OH)_2$ layer was also directly grown

on the treated Ni foam via an electrodeposition process[16]. The electrolyte used for

electrodeposition was 0.05 M $Co(NO_3)_2$. The electrodeposition was carried out in a

three-electrode electrochemical cell by cyclic voltammetry for 30 cycles over a

potential range of -1.2 to -0.8 V vs. Ag/AgCl at a scan rate of 50 mV s-1. The mass

loading of $Co(OH)_2$ on Ni foil is 1.5 mg cm-2. Photographs of $Co(OH)_2$, Ni_3S_2 and

$Ni_3S_2@Co(OH)_2$ are shown in Figure S1.

## 2.2. Physical characterization

X-ray diffraction analysis was carried out on Shimadzu XD-3A with Cu-Kα

radiation and the scan rate is set to 10° min-1. The morphology of the as-prepared

materials was investigated by scanning electron microscopy (SEM, Carl Zeiss Ultra

Plus Electron Microscope) and scanning transmission electron microscopy (STEM,

JEM-2000 FX). X-ray photoelectron spectroscopy (XPS) spectra were analyzed on

PHI-5702 spectrometer and were referenced to the C 1*s* peak at 285.0 eV.

2.3. Electrochemical characterization

6

The electrochemical tests were carried out in a three-electrode electrochemical cell connected to a potentiostat/galvanostat (CHI 660, CH Instruments, Inc., Shanghai), using graphite rod, Hg/HgO and the *as*-prepared catalysts as the counter electrode, the reference electrode and the working electrode (1×1 cm^2) respectively. Linear sweep voltammetry (LSV) and cyclic voltammetry (CV) were carried out in aqueous KOH electrolyte (1.0 M). Electrochemical impedance spectrum was measured from 0.01 to 1,000,000 Hz for the HER and the OER at corresponding potentials. To evaluate the electrochemical performance for the overall water splitting, $Ni_3S_2@Co(OH)_2$ electrodes was used as both the cathode and anode in a water electrolyzer. *iR* compensation (90%) was used for all the electrochemical experiments.

3. Results and discussion
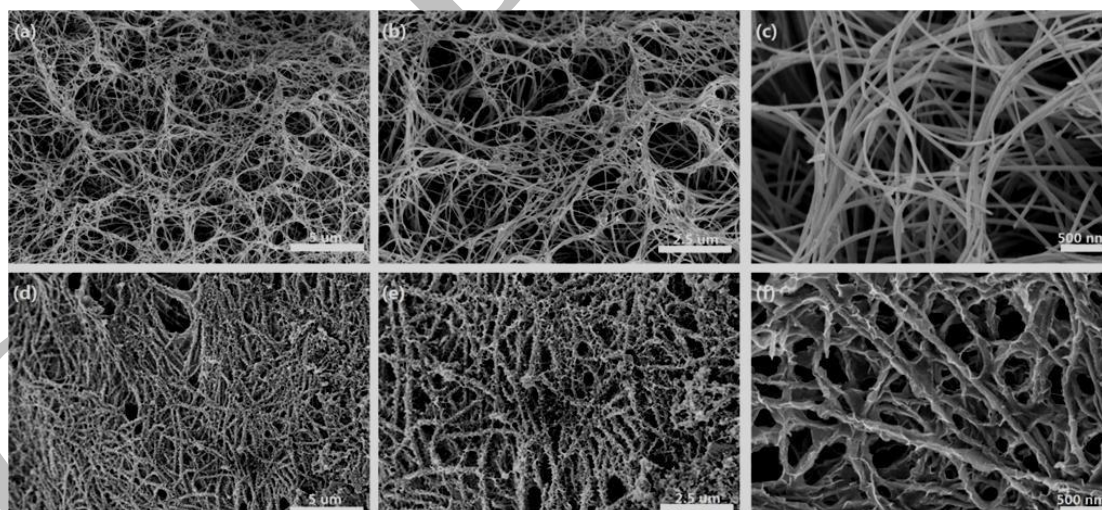
Figure 1. (a, b, c) SEM images of 1-*D* Ni_3S_2; (d, e, f) 1-*D* $Ni_3S_2@Co(OH)_2$.

During the synthesis of the 1-*D* $Ni_3S_2@Co(OH)_2$ nanowires, 1-*D* Ni_3S_2 was firstly grown onto the surface of Ni foam via a solvothermal method, in which S powder was used as the sulfur source and Ni foam as the Ni source. In this method, $Co(OH)_2$ layer

7

was successfully formed on the 1-*D* Ni_3S_2. Due to the high electrical conductivity of

Ni_3S_2 nanowires [25], $Co(OH)_2$ layer coated on them could facilitate the electron

transfer between $Co(OH)_2$ and Ni_3S_2 during the electrochemical processes, which

could result in good electrochemical performance. The morphology of the Ni_3S_2 and

$Ni_3S_2@Co(OH)_2$ were firstly evaluated by scanning electron microscopy (SEM).

Hair-like nanowires were observed in Figure 1(a-c), namely the obtained Ni_3S_2

nanowires are thin and long with a uniform diameter. These 1-*D* nanowires were

interconnected with each other and formed a 3-*D* network. From the SEM images, it

can be observed that only nanowires and no other shapes of particles were formed,

indicating that this solvothermal method was an efficient strategy for synthesizing

Ni_3S_2 nanowires. Moreover, it was found that the $Co(OH)_2$ layer was further grown

onto the Ni_3S_2 nanowires hydrothermally. The morphology of the 1-*D* nanowires was

retained (Figure 1(d-e)), but the surface of the obtained nanowires became very rough

with small particles coated onto them. It can be noted that the surface of Ni_3S_2

nanowires was evenly coated by sheet-like layer and no other shaped particles were

found in Figure 1(e). Finally, Figure 1 shows that hierarchical structures were formed

during the synthesis, i.e. 1-*D* nanowires, 2-*D* nanosheets, and 3-*D* networks were

produced. Such unique structures could generate more active sites for electrochemical

processes, and further result in improved electrochemical properties.

The crystal structure of the obtained $Ni_3S_2@Co(OH)_2$ was evaluated by X-ray

diffraction analysis. There are three strong diffraction peaks at 44.6_o, 51.7_o and 76.5_o

corresponding to the nickel arose from the Ni foam (Figure 2(a)). The figure also

8

shows the main characteristic diffraction peaks of Ni_3S_2 (JCPDS Card No.44-1418)

and $Ni_3S_2@Co(OH)_2$, i.e. the peaks at ca. 21.6_o, 31.4_o, 38.2_o, 49.9_o, and 54.9_o

correspond to the (101), (110), (003), (113) and (122) planes respectively. This

finding indicates that Ni_3S_2 phase was grown on the Ni. Moreover, no peaks related to

other nickel sulfides and oxides were observed in Figure 2(a); in other words, only

pure Ni_3S_2 phase was formed on Ni foam. According to the JCPDS No.46-0605,

major characteristic peaks of α-$Co(OH)_2$ were found in Figure 2(a). It was also found

that the intensity of these peaks related to α-$Co(OH)_2$ was very low, suggesting that

the α-$Co(OH)_2$ formed on Ni_3S_2 had a very low crystallinity. It was previously

reported that α-$Co(OH)_2$ is a hydrotalcite-like structure composed by positively

charged $Co(OH)_{2-x}(OH)_x$ layers in which balancing anions are stored between the

hydroxide layers [29]. Due to its large interlayer distance, the α-$Co(OH)_2$ material is

recognized as a better electrode material than β-$Co(OH)_2$ [28]. It can be then

stipulated that the sheet-like α-$Co(OH)_2$ with large interlayer distance could keep

more electrolyte ions and facilitate the ion transfer during the electrochemical

processes.

Transmission electron microscopy (TEM) was also applied to investigate the

detailed microstructure of $Ni_3S_2@Co(OH)_2$. It shows that the Ni_3S_2 nanowires with

diameters of ca. 50 nm were wrapped around by the $Co(OH)_2$ thin and wrinkled

nanosheets (Figure 2(b)). Furthermore, no other forms of $Co(OH)_2$ particles were

found, an observation that is agreed well with the XRD and SEM results. The part in

the red rectangle in Figure 2(b) was further zoomed-in and presented in Figure 2(c).

As shown by the red line in Figure 2(c), there is a blur boundary between $Co(OH)_2$ and Ni_3S_2 phases, indicative of the intimate contact between these two phases. Well-defined lattice fringes with a *d*-spacing distance of 0.27 nm corresponding to the (100) plane of α-$Co(OH)_2$ [29] and 0.28 nm to the (110) plane of Ni_3S_2 [30] were observed in the high-resolution TEM image (Figure 2(d)). This finding further confirms that α-$Co(OH)_2$ was formed on Ni_3S_2 nanowires. $Ni_3S_2@Co(OH)_2$ was further confirmed by the Scanning TEM (STEM) image (Figure 2i). Electron energy-loss spectroscopic mapping (Figure 2(f–i)) shows uniform distribution of Ni and S elements and the presence of Co and O indicates the $Co(OH)_2$ phase existed on the surface, further demonstrating the core-shell structure of the $Ni_3S_2@Co(OH)_2$.
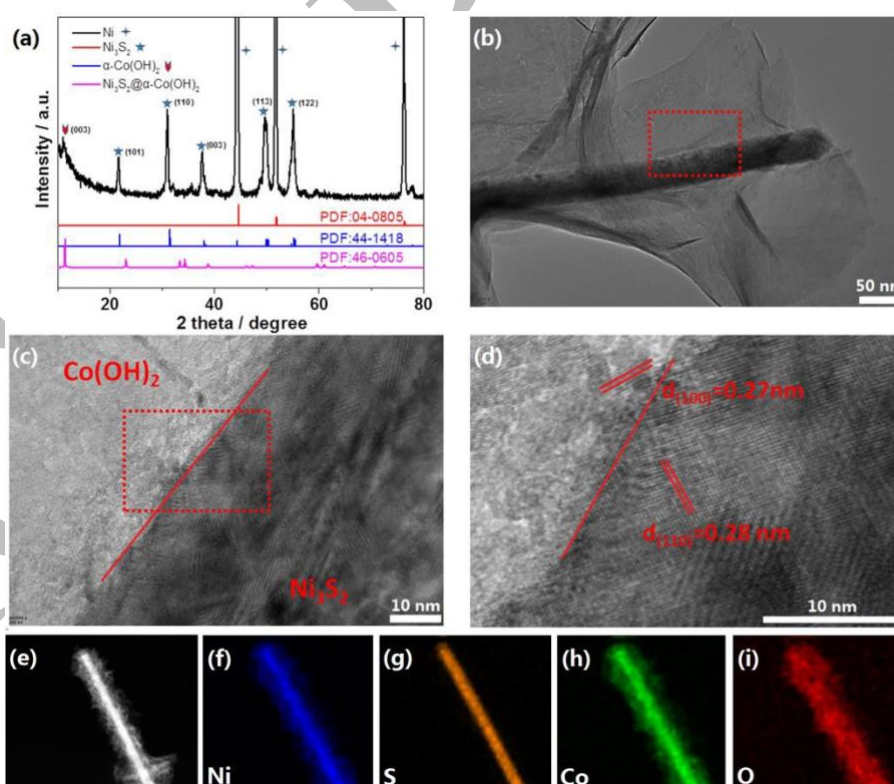
Figure 2. XRD patterns (a) , TEM images of $Ni_3S_2@Co(OH)_2$ (b, c, d) and STEM

10

In the XPS spectrum shown in Figure S2(a), the signals of Co, Ni, S and O were detected, suggesting that there are Co, Ni, O and S elements in the obtained electrode. The XPS spectrum of Ni $2p$ (Figure S2(b)) exhibits two major peaks at 855.7 eV and 873.1 eV, which can correspond to Ni $2p_{3/2}$ and Ni $2p_{1/2}$ respectively, with two satellites at 879.5 eV and 861.4 eV, attributed to the Ni^{2+} and Ni^{3+} [31]. As shown in Figure S2(c), two peaks (at 162.1 and 163.3 eV), accompanied by a satellite peak (at 168.0 eV) result from sulfur in the electrode. The Co $2p$ spectrum of $Ni_3S_2@Co(OH)_2$ can be deconvoluted into two spin-orbit doublets (Figure S2(c)), i.e. into Co $2p_{1/2}$ and Co $2p_{3/2}$, accompanied with two shake-up satellites, corresponding to the binding energies for Co^{2+} [32]. The binding energy gaps of Co $2p_{1/2}$ and Co $2p_{3/2}$ were found to be 16.0 eV, which further confirmed that Co^{2+} was present in $Co(OH)_2$ [22].
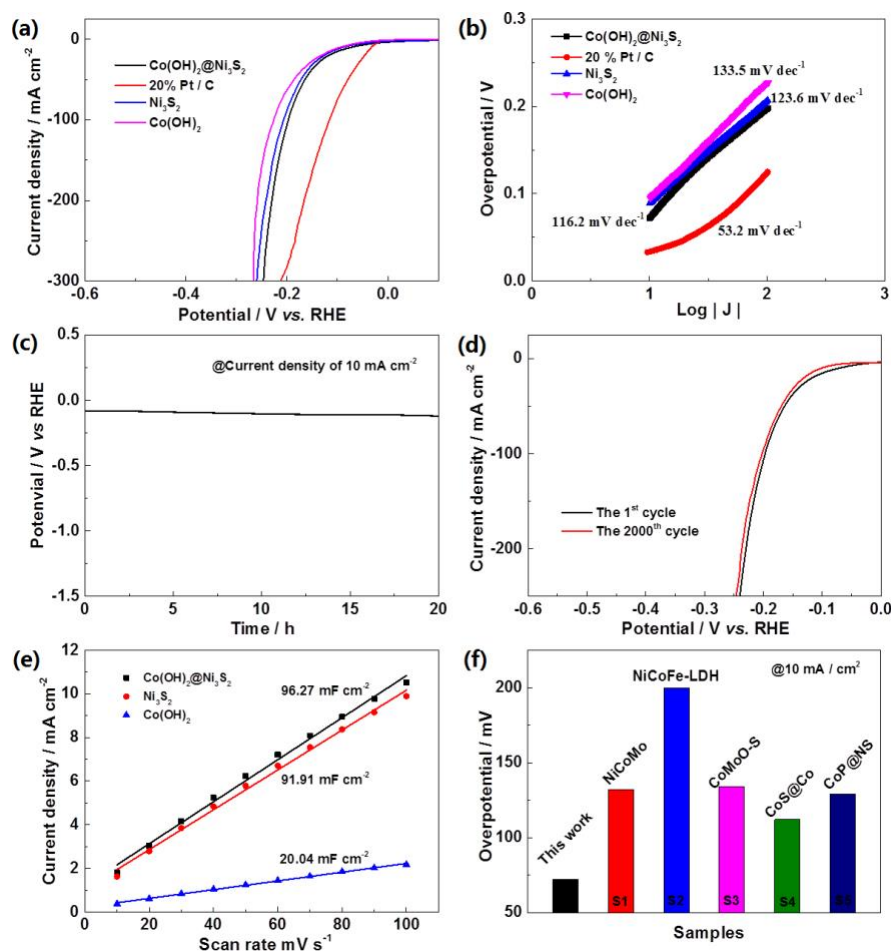
11

Figure 3. (a) Linear sweep voltammogram (LSV) curves (5 mV s^{-1}) for HER tested in aqueous KOH electrolyte (1.0 M); (b) Tafel plots; (c) Chronopotentiometry measurement of HER at 10 mA cm^{-2}; (d) HER LSV curves of the 1st and 2,000th cycles; (e) Linear fitting of Δj ($\Delta j = j_a - j_c$) vs. scan rates at a potential of +0.42 V *vs.* RHE; (f) the overpotential at $j = 10$ mA cm^{-2} compared with the values reported in the literature.

The HER electrocatalytic performances of as-prepared electrodes were initially measured by LSV in a 1.0 M KOH solution and compared with the Pt/C (20 wt. %), the state-of-the-art commercial HER catalysts. The HER onset potentials and overpotentials at 10 mA.cm^{-2} are critical parameters for evaluating the HER activity.

12

The HER onset potentials measured at 10 mA cm^{-2} for Ni_3S_2, $Co(OH)_2$, $Ni_3S_2@Co(OH)_2$ and Pt/C were found to be +89, +95, +72, +33 mV *vs.* RHE respectively (Figure 3(a)). Among all the tested samples, the Pt/C sample has the lowest onset potential. It was also found that the onset potential of $Ni_3S_2@Co(OH)_2$ was lower than the two other samples, in other words, by introducing $Co(OH)_2$ on Ni_3S_2 could effectively improve the HER activity. In order to shed light on the HER mechanism(s) on these new catalysts, Tafel plots were generated as shown in Figure 3(b). In this study, Tafel slopes were calculated using Equation 1:

$$\eta = b \log j + a \qquad (1)$$

where *b* is the Tafel slope, *η* the overpotential and *j* the current density.

The Tafel slopes of Ni_3S_2, $Co(OH)_2$, $Ni_3S_2@Co(OH)_2$ and Pt/C were calculated to be 123.6, 133.5, 116.2 and 53.2 mV dec^{-1} respectively (Figure 3(b)), implying that the HER reaction on $Ni_3S_2@Co(OH)_2$ was faster than the reaction on Ni_3S_2 and $Co(OH)_2$, but lower than that of Pt/C. In general, electrocatalytic HER in basic solutions proceeds in two steps. The first is a primary discharge step (Volmer reaction: $H_2O + e^- \rightarrow H_{ads} + OH^-$) and the second is either an electrochemical desorption step (Heyrovsky reaction: $H_2O + H_{ads} + e^- \rightarrow H_2 + OH^-$) or a recombination one (Tafel reaction: $H_{ads} + H_{ads} \rightarrow H_2$). Both pathways involve the adsorption of H_2O molecules on the empty active sites, electrochemical reduction of adsorbed water into adsorbed hydrogen atoms (H_{ads}) and hydroxyl ions (OH^-), desorption of OH^- to refresh the catalyst surface and formation of H_{ads} for H_2 evolution [33, 34]. For the $Ni_3S_2@Co(OH)_2$ sample, the HER occurred as a *Volmer-Heyrovsky process*, in which

13

the rate-determining process is the electrochemical desorption. In the case of Ni_3S_2

and $Co(OH)_2$, the HER mechanism followed the lowly efficient *Volmer process*. The

Tafel slopes further indicated that the $Co(OH)_2$ formed on 1-*D* Ni_3S_2 could efficiently

improve the HER process occurring on its surface. Chronopotentiometry experiments

were conducted to investigate the HER at 10 mA cm^{-2}. As shown in Figure S4(a), the

EIS tests are used to examine the ion transfer kinetics under HER operating

conditions. The charge-transfer resistance of the $Ni_3S_2@Co(OH)_2$ is much lower than

that of Ni_3S_2 and $Co(OH)_2$, which further confirms the excellent ion transfer kinetics

of the $Ni_3S_2@Co(OH)_2$. The overpotential of $Ni_3S_2@Co(OH)_2$ only increased by +37

mV after 20 h of a continuous test at a current density of 10 mA cm^{-2} (Figure 3(c)),

indicating that $Ni_3S_2@Co(OH)_2$ is stable in HER. The HER durability is an important

criterion for the HER performance; LSV experiments were thus carried out

continuously on $Ni_3S_2@Co(OH)_2$ and Figure 3(d) is the LSV plots of the 1st and

2,000th cycles. After 2,000 cycles, the overpotential of $Ni_3S_2@Co(OH)_2$ positively

shift 30 mV, which is similar in value to the commercial Pt/C sample (Figure S3).

This finding indicates that the $Ni_3S_2@Co(OH)_2$ catalyst material possesses good HER

stability. Electrochemical double-layer capacitance (EDLC) was employed to

calculate the electrochemical surface area (ECSA) via CV analysis. A potential

window of 0.36-0.46 V was chosen in order to avoid the *Faradic reaction* during CV

testing (Figure S4(b-d)). The Δj ($\Delta j = j_a - j_c$) *vs.* scan rates (v) at +0.42 V *vs.* RHE

was plotted (Figure 3(e)). The slopes of these straight lines represent the EDLC. The

EDLC values of Ni_3S_2, $Co(OH)_2$ and $Ni_3S_2@Co(OH)_2$ samples were found to be

14

91.91, 20.04 and 96.27 mF cm-2 respectively, indicating that more electrochemically

active sites available on Ni3S2@Co(OH)2 than other two samples. The overpotential

of Ni3S2@Co(OH)2 at 10 mA cm-2 was 72 mV (Figure 3(f)). Although it is lower than

Pt/C, this overpotential is higher than many reported Ni or Co-based HER
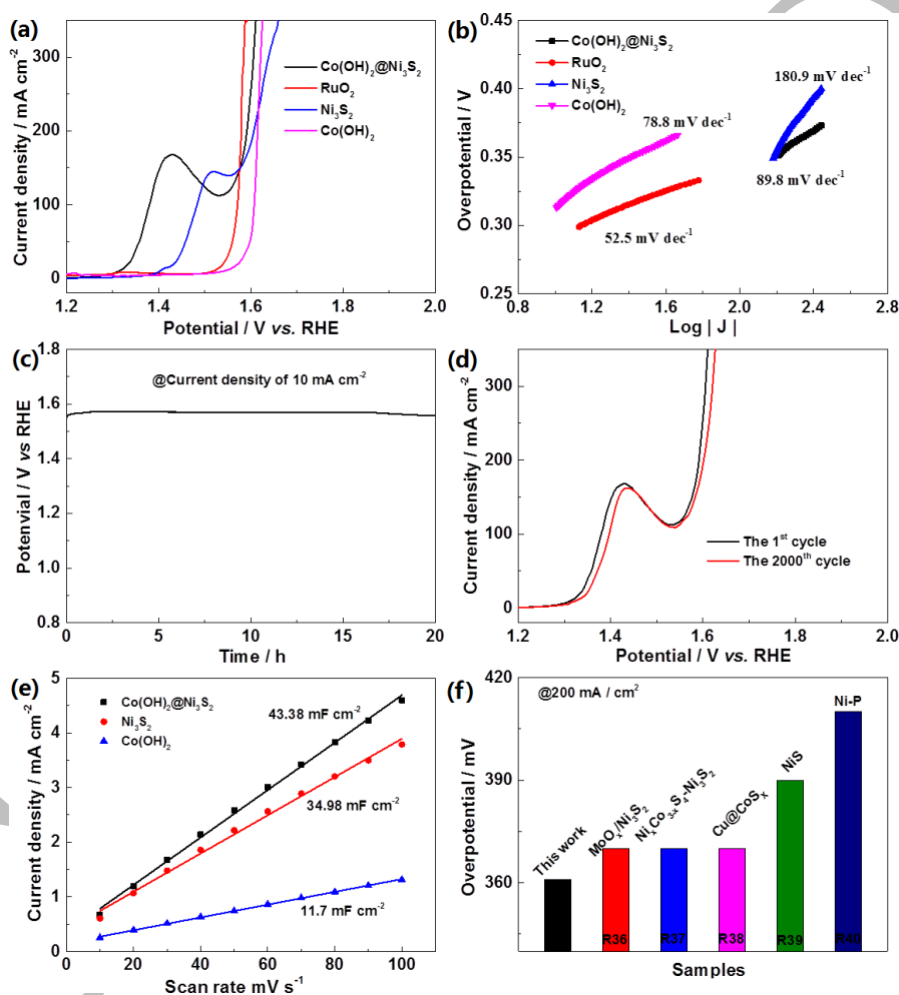
electrocatalysts listed in Figure 3(f) and Table S1.

Figure 4. (a) OER LSV curves obtained in aqueous KOH solution (1.0 M); (b) Tafel

plots; (c) Chronopotentiometry of OER at 10 mA.cm-2; (d) OER LSV curves of the 1st

and 2,000th cycles; (e) Electrochemical double-layer capacitance (EDLC); (f)

Comparison of overpotentials at 10 mA cm-2 with values reported in literature.

The OER electrochemical activity was evaluated by LSV in aqueous KOH solution

(1.0 M) and compared with RuO_2 (Figure 4(a)). From previous studies on Ni-based

catalysts, an oxidation peak at +1.4-+1.5 V *vs.* RHE was observed and attributed to

the oxidation of Ni_{+2} to Ni_{+3} [35]. Because of this oxidation peak, it was difficult to

compare the onset potentials of the *as*-prepared samples. Based upon the LSV curves

shown in Figure 4(a), the overpotentials of RuO_2 and $Ni_3S_2@Co(OH)_2$ at 200

$mA.cm_{-2}$ were calculated to be 350 mV and 361 mV respectively, which are higher

than two other *as*-prepared electrodes. OER electrocatalytic activity was also

evaluated by the Tafel plot for all the samples. Thus as shown in Figure 4(b),

$Ni_3S_2@Co(OH)_2$ has a higher OER activity than Ni_3S_2. Long-term stability was also

conducted by chronopotentiometry at 200 mA cm_{-2} in a 1.0 KOH solution (Figure

4(c)). The charge-transfer resistance of the $Ni_3S_2@Co(OH)_2$ is much lower than the

Ni_3S_2 and the $Co(OH)_2$ (Figure S6(a)), which further confirms that $Ni_3S_2@Co(OH)_2$

has a better charge-transfer kinetics. At 10 mA cm_{-2}, the $Ni_3S_2@Co(OH)_2$ could

deliver a constant potential of 1.56 V for 20 h without any obvious decay, confirming

its good electrocatalytic stability towards the OER. LSV cycling experiments were

also carried out to investigate the OER stability for the $Ni_3S_2@Co(OH)_2$ sample. The

LSV curves (1_{st} and $2,000_{th}$ cycles) are presented in Figure 4(d) and the corresponding

LSV curves of RuO_2 in Figure S5. The overpotential of $Ni_3S_2@Co(OH)_2$ increased by

+18 mV, lower than that of RuO_2 (+45 mV), further confirming its OER stability in

weak KOH solution. The electrochemical surface areas for the OER were also

evaluated by the EDLC (Figure 4(e)). It is found that the $Ni_3S_2@Co(OH)_2$ has the

highest EDLC among the three samples; in other words, $Ni_3S_2@Co(OH)_2$ had more electrochemical active sites than the other two samples. The overpotential of $Ni_3S_2@Co(OH)_2$ (10 mA cm-2) was also benchmarked against many representative Ni and Co-based OER catalysts in Figure 4(f) [36-40] and Table S2. It was observed that the $Ni_3S_2@Co(OH)_2$ material exhibited the highest OER activity.

Since the $Ni_3S_2@Co(OH)_2$ possesses a very good HER/OER catalytic activity and stability, a two-electrode water electrolyzer containing the $Ni_3S_2@Co(OH)_2$ catalyst material on both the cathode and anode was assembled, to investigate the electrochemical performance in the real-world condition. Figure 5(a) is the polarization curves of $Ni_3S_2@Co(OH)_2$||$Ni_3S_2@Co(OH)_2$ (N||N) and Pt/C||RuO_2. It was found that the N||N electrolyzer could deliver a cell voltage of 1.70 V at100 mA cm-2, a value slightly larger than Pt/C||RuO_2 cell (1.622 V). When the current of N||N was set at 10 mA cm-2, N||N produced a stable cell voltage of 1.64 V for more than 20 h, suggesting that the obtained $Ni_3S_2@Co(OH)_2$ is electrocatalytically stable for the overall water splitting. The N||N was benchmarked with several transitional metal-based bifunctional HER and OER catalysts in Figure 5(c) and Table S3, and the comparison showed that $Ni_3S_2@Co(OH)_2$ possesses outstanding catalytic activity under water electrolyzer conditions. As shown in Figure S7(a), the durability of N||N was also tested by continuous LSV cycles. It was observed that the overpotential of N||N cell only increased by +15 mV at 10 mA cm-2, comparable to the stability of Pt/C||RuO_2 electrolyzer (+36 mV at 10 mA cm-2) (Figure S7(b)). The N||N was also connected to a desktop wind turbine (Figure 5(d)) to generate hydrogen and oxygen

using a renewable energy source. As we can see from the video, the surface of the electrode began to produce bubbles gradually with the fan. It was clearly observed that many bubbles were formed on both the cathode and anode when the miniature wind turbine started to generate electricity, further demonstrating the highly electrocatalytic HER and OER activity of $Ni_3S_2@Co(OH)_2$ and its great potential for use in water electrolyzer to produce hydrogen from renewable energy sources.
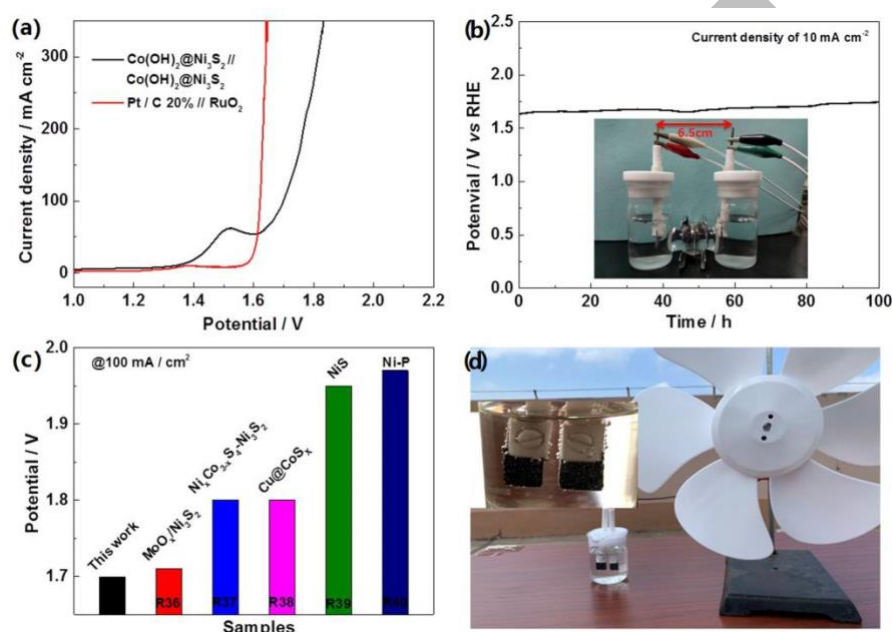

Figure 5.(a) polarization curve for the overall water splitting; (b) chronopotentiometry analyses at 10 mA cm-2; (c) potentials comparison at 10 mA cm-2; (d) picture of water splitting with a desktop wind turbine.

4. Conclusions

In this study, Ni_3S_2 nanowires were synthesized and wrapped around by ultrathin α-$Co(OH)_2$ layer which was directly fabricated on Ni foam by solvothermal method. Since the ultrathin α-$Co(OH)_2$ layer was formed on 1-*D* Ni_3S_2 nanowires, the obtained $Ni_3S_2@Co(OH)_2$ exhibited excellent HER and OER electrocatalytic performance in

18

terms of decreased onset potential, decreased overpotential and increased durability.

The high HER and OER performance were also demonstrated by using the

$Ni_3S_2@Co(OH)_2$ as HER and OER bifunctional catalyst in the water electrolyzer,

delivering a constant voltage of 1.64 V at the current density of 10 mA cm^{-2} for 100 h.

This finding indicated that the obtained $Ni_3S_2@Co(OH)_2$ was electrocatalytically

stable during the overall water splitting. Due to its high HER/OER activity and

stability in KOH electrolyte, $Ni_3S_2@Co(OH)_2$ suggests that it could be used as a

promising and alternative bifunctional electrocatalyst material for alkaline water

electrolyser.

Acknowledgment

References

[1] C. Lv, Q. Yang, Q. Huang, Z. Huang, H. Xia, C. Zhang, J. Mater. Chem. A, 4 (2016) 13336-13343.

[2] Q. Liu, L. Xie, F. Qu, Z. Liu, G. Du, A.M. Asiri, X. Sun, Inorg Chem Front, 4 (2017) 1120-1124.

[3] P. Li, R. Zhao, H. Chen, H. Wang, P. Wei, H. Huang, Q. Liu, T. Li, X. Shi, Y. Zhang, M. Liu, X. Sun, Small, 15 (2019) 1805103.

[4] X. Xu, Y. Zhong, Z. Shao, Trends in Chemistry, 1 (2019) 410-424.

[5] J. Ding, S. Ji, H. Wang, H. Gai, F. Liu, B.G. Pollet, R. Wang, Chem Commun, 55 (2019) 2924-2927.

[6] R.M. Yadav, J. Wu, R. Kochandra, L. Ma, C.S. Tiwary, L. Ge, G. Ye, R. Vajtai, J. Lou, P.M. Ajayan, ACS Appl Mater Inter, 7 (2015) 11991-12000.

[7] X. Cheng, H. Wang, M. Ming, W. Luo, Y. Wang, Y. Yang, Y. Zhang, D. Gao, J. Bi, G. Fan, ACS Sustain Chem Eng, 6 (2018) 11487-11492.

[8] S. Anantharaj, K. Karthick, M. Venkatesh, T.V.S.V. Simha, A.S. Salunke, L. Ma, H. Liang, S. Kundu, Nano Energy, 39 (2017) 30-43.

[9] Z. Wang, J. Li, X. Tian, X. Wang, Y. Yu, K.A. Owusu, L. He, L. Mai, ACS Appl Mater Inter, 8 (2016) 19386-19392.

[10] T. Liu, L. Xie, J. Yang, R. Kong, G. Du, A.M. Asiri, X. Sun, L. Chen, ChemElectroChem, 4 (2017)

1840-1845.

[11] L. Xie, F. Qu, Z. Liu, X. Ren, S. Hao, R. Ge, G. Du, A.M. Asiri, X. Sun, L. Chen, J. Mater. Chem. A, 5 (2017) 7806-7810.

[12] X. Xu, C. Su, W. Zhou, Y. Zhu, Y. Chen, Z. Shao, Adv Sci (Weinh), 3 (2016) 1500187.

[13] X. Xu, Y. Chen, W. Zhou, Y. Zhong, D. Guan, Z. Shao, Adv Mater Inter, 5 (2018) 1701693.

[14] Q. Liu, L. Xie, Z. Liu, G. Du, A.M. Asiri, X. Sun, Chem commun, 53 (2017) 12446-12449.

[15] X. Du, Z. Yang, Y. Li, Y. Gong, M. Zhao, J. Mater. Chem. A, 6 (2018) 6938-6946.

[16] Z. Wang, S. Ji, F. Liu, H. Wang, X. Wang, Q. Wang, B.G. Pollet, R. Wang, ACS Appl Mater Inter, 11 (2019) 29791-29798.

[17] S.M. Tan, C.K. Chua, D. Sedmidubsky, Z.C. Sofer, M. Pumera, Phys. Chem. Chem. Phys., 18 (2016) 1699-1711.

[18] F. Ming, H. Liang, H. Shi, X. Xu, G. Mei, Z. Wang, J. Mater. Chem. A, 4 (2016) 15148-15155.

[19] Y. Kou, J. Liu, Y. Li, S. Qu, C. Ma, Z. Song, X. Han, Y. Deng, W. Hu, C. Zhong, ACS Appl Mater Inter, 10 (2018) 796-805.

[20] S. Bai, C. Wang, M. Deng, M. Gong, Y. Bai, J. Jiang, Y. Xiong, Angew. Chem., 53 (2014) 12120-12124.

[21] P. Guo, J. Wu, X.-B. Li, J. Luo, W.-M. Lau, H. Liu, X.-L. Sun, L.-M. Liu, Nano Energy, 47 (2018) 96-104.

[22] Y. Jiang, X. Li, T. Wang, C. Wang, Nanoscale, 8 (2016) 9667-9675.

[23] Y. Luo, X. Li, X. Cai, X. Zou, F. Kang, H.M. Cheng, B. Liu, ACS Nano, 12 (2018) 4565-4573.

[24] C. Zhao, F. Ren, X. Xue, W. Zheng, X. Wang, L. Chang, J. Electroanal. Chem., 782 (2016) 98-102.

[25] C. Fangshuai, J. Shan, L. Quanbing, W. Hui, L. Hao, B.D.J. L., W. Guoxiu, W. Rongfang, Small, 14 (2018) 1800791.

[26] H. Chen, J. Jiang, L. Zhang, H. Wan, T. Qi, D. Xia, Nanoscale, 5 (2013) 8879-8883.

[27] F. Chen, H. Wang, S. Ji, B.G. Pollet, R. Wang, J Alloy Compd, 785 (2019) 684-691.

[28] Y.M. Hu, M.C. Liu, Y.X. Hu, Q.Q. Yang, L.B. Kong, W. Han, J.J. Li, L. Kang, Electrochim. Acta, 190 (2016) 1041-1049.

[29] Y. Wang, D. Yan, S. El Hankari, Y. Zou, S. Wang, Adv Sci (Weinh), 5 (2018) 1800064.

[30] X. Shang, J.Q. Chi, Z.B. Wang, B. Dong, J.C. Zhao, X.H. Li, K.L. Yan, L. Wang, Y.M. Chai, C.G. Liu, J Catal, 368 (2018) 112-119.

[31] J. Ding, S. Ji, H. Wang, V. Linkov, H. Gai, F. Liu, Q. Liu, R. Wang, ACS Sustain Chem Eng, 7 (2019) 3974-3981.

[32] G. He, M. Qiao, W. Li, Y. Lu, T. Zhao, R. Zou, B. Li, J.A. Darr, J. Hu, M.M. Titirici, Adv Sci, 4 (2017) 1600214.

[33] X. Xu, Y. Chen, W. Zhou, Z. Zhu, C. Su, M. Liu, Z. Shao, Adv Mater, 28 (2016) 6442-6448.

[34] W. Zhu, R. Zhang, F. Qu, A.M. Asiri, X. Sun, ChemCatChem, 9 (2017) 1721-1743.

[35] Y. Rao, H. Ning, X. Ma, Y. Liu, Y. Wang, H. Liu, J. Liu, Q. Zhao, M. Wu, Carbon, 129 (2018) 335-341.

[36] Y. Wu, G.-D. Li, Y. Liu, L. Yang, X. Lian, T. Asefa, X. Zou, Adv Func Mater, 26 (2016) 4839-4847.

[37] Y. Wu, Y. Liu, G.-D. Li, X. Zou, X. Lian, D. Wang, L. Sun, T. Asefa, X. Zou, Nano Energy, 35 (2017) 161-170.

[38] Y. Liu, Q. Li, R. Si, G.D. Li, W. Li, D.P. Liu, D. Wang, L. Sun, Y. Zhang, X. Zou, Adv Mater, 29 (2017).

[39] W. Zhu, X. Yue, W. Zhang, S. Yu, Y. Zhang, J. Wang, J. Wang, Chem commun, 52 (2016) 1486-1489.

[40] Q. Liu, S. Gu, C.M. Li, Journal of Power Sources, 299 (2015) 342-346.

Video
Click here to download Video: VIDIO.mp4

Declaration of Interest Statement

I declare that this manuscript has not been submitted to other journals and there is no conflict of interest for this manuscript and that its submission is approved by all authors and tacitly or explicitly by the responsible authorities where the work was carried out. If accepted, it will not be published elsewhere in the same form, in English or in any other language, without the written consent of the publisher.

Yours faithfully

Prof. Rongfang Wang

Qingdao University of Science and Technology